Interatomic potential-based semiclassical theory for Lennard-Jones fluids

A. V. Raghunathan, J. H. Park, and N. R. Aluru[a)]
Beckman Institute for Advanced Science and Technology, University of Illinois at Urbana-Champaign, Urbana, Illinois 61801, USA

(Received 3 July 2007; accepted 10 September 2007; published online 1 November 2007)

An interatomic potential based semiclassical theory is proposed to predict the concentration and potential profiles of a Lennard-Jones (LJ) fluid confined in a channel. The inputs to the semiclassical formulation are the LJ parameters of the fluid and the wall, the density of channel wall atoms, and the average concentration of the fluid inside the channel. Using the semiclassical formulation, fluid confinement in channel with widths ranging from $2\sigma_{ff}$ to $100\sigma_{ff}$, where σ_{ff} is the fluid-fluid LJ distance parameter, is investigated. The concentration and potential predicted by the semiclassical formulation are found to be in good agreement with those from equilibrium molecular dynamics simulations. While atomistic simulations in large channels are computationally expensive, the proposed semiclassical formulation can rapidly and accurately predict the concentration and potential profiles. The proposed semiclassical theory is thus a robust and fast method to predict the interfacial and "bulk" fluid phenomena in channels with widths ranging from the macroscale down to the scale of a few atomic diameters. © *2007 American Institute of Physics*.
[DOI: 10.1063/1.2793070]

I. INTRODUCTION

There is currently growing interest in designing micro and nanofluidic channels for applications in lab-on-a-chip, energy storage and conversion, water purification, and nanomanufacturing.[1–3] Computational analysis plays an important role in design and optimization of these micro and nanofluidic devices; numerous studies have already been performed to model and predict the static and dynamic properties of fluids in micro and nanochannels.[4] Continuum or classical theories are generally accurate in predicting properties and transport of bulk fluids where nanoscale confinement and interfacial behavior are not significant. When the fluid is under strong confinement, i.e., a bulk description of the fluid is not valid, atomistic molecular dynamics (MD) simulations[5] can be used to understand the fluid behavior. There are many examples where both the interfacial behavior and the bulk behavior of the fluid can be important. For example, hybrid micro-nanochannels, where ion selective nanochannels are connected to microscale solution chambers, require proper understanding of both the bulk and confined behavior of the fluid. Another example where both the macroscale and the atomistic features become important is in electro-osmosis through channels with an electric-double layer (EDL).[6] In this case, the strong density gradients of the electrolyte produced in the atomic scale are coupled to the macroscopic behavior in ways that are difficult to capture by classical constitutive relations or other average descriptions. In micro and nanofluidic devices where both the interfacial behavior and the macroscopic behavior of the fluid are important, the use of a classical continuum theory to resolve the physics in the entire device can be inaccurate, while the use of MD simulations may not be possible because of computational limitations. Hence, it is of fundamental interest to develop methods that combine the atomistic features with the existing continuum theory. Approaches that seek to accomplish this are broadly described as multiscale models.[7] Multiscale models aim at providing a "bridge" between the atomistic and continuum theories, either by simultaneously simulating them in different regions of the domain or by incorporating the atomistic physics that is missing in the classical theories.[8]

The multiscale simulations developed to understand flow under confinement can be categorized into coupled continuum methods[9,10] involving either a heterogeneous domain decomposition or a corrected continuum theory, and coarse-grained methods, which involve reducing the degrees of freedom in a microscopic Hamiltonian.[11,12] A hydrodynamic model used for this purpose is the dissipative particle dynamics (DPD) approach,[13,14] which considers a "cluster" of atoms as a particle interacting with other such cluster particles with a distinct dissipative field of interaction. DPD suffers from the drawback that the results of the simulation depend on the optimally chosen time step. Further, the integration scheme to be chosen is a nontrivial task and could lead to artifacts in the predicted results.[15] Also, the boundary conditions applied in DPD are not well defined; ongoing studies involve finding approaches to improve the applied boundary conditions.[16] Other approaches to study fluids under confinement involve theoretical predictions, e.g., using the integral density functional theory (DFT) theory[17] to predict the fluid dynamics in the system by solving modified continuum equations with a predicted density. Though the mathematical framework of DFT is formally exact, a precise expression of the intrinsic Helmholtz energy as a functional of the molecular density profile is unknown for most systems of practical

[a)]Author to whom correspondence should be addressed. Electronic mail: aluru@uiuc.edu

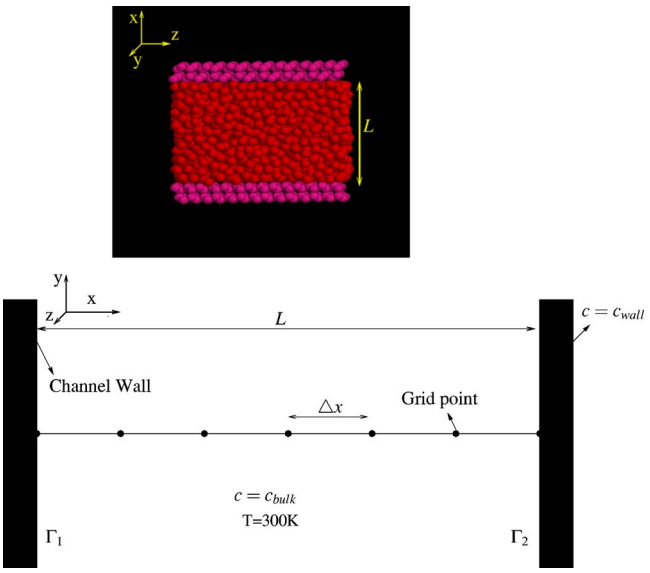

FIG. 1. (Color online) Molecular representation (top) and a continuum representation (bottom) of a Lennard-Jones fluid confined between two channel walls.

interest.[18] Further details of confined fluid theories including DFT can be found in Refs. 18 and 19 and references therein.

In this study, we propose a novel interatomic potential-based semiclassical theory to predict the concentration and potential profiles of LJ fluids confined in channels of widths ranging from $2\sigma_{ff}$ to $100\sigma_{ff}$ (σ_{ff} is the fluid-fluid LJ parameter). For each of the channels studied, comparisons are made with MD simulations to analyze the accuracy of the proposed formulation. The results obtained from the formulation are found to be in good agreement with the MD simulation data. To our knowledge, this is the first semiclassical formulation that, while preserving the atomistic physics close to the wall, quickly and accurately predicts the concentration and potential for a wide range of channel widths. Hence, the proposed semiclassical formulation is a robust, fast, and accurate method that can be used to predict the atomistic details at various length scales ranging from the nanoscale to the macroscale.

The remainder of the paper is outlined as follows. In Sec. II, we describe the semiclassical theory along with the details on computing the wall-fluid and fluid-fluid potentials, the governing equation that is used to solve the multiscale formulation, and a description of the multiscale algorithm. Simulation details on MD and semiclassical formulation are given in Sec. III. In Sec. IV, we discuss at length the results obtained from the semiclassical formulation and compare them with MD data for a wide range of channels. Finally, conclusions are presented in Sec. V.

II. THEORY

We derive a new interatomic potential-based continuum formulation (defined here as the semiclassical theory) for a LJ fluid confined between two solid walls that are infinite in the y- and z-directions (see Fig. 1). Therefore, it is reasonable to assume a one-dimensional variation of the concentration of the fluid across the channel while deriving the semiclassical formulation. For the derivation of the semiclassical theory, we assume that the average concentration of the LJ fluid inside the channel, c_{avg}, and the wall-atom concentration, c_{wall}, are given. Our goal is to calculate the concentration and potential profile across the channel using the proposed semiclassical formulation. If the total potential profile, U, in the channel is known, the fluid concentration, c, inside the channel can then be obtained by solving the well known 1D steady-state Nernst-Planck equation,[20] i.e.,

$$\frac{d}{dx}\left(\frac{dc}{dx}+\frac{c}{RT}\frac{dU}{dx}\right)=0, \tag{1}$$

where R is the gas constant, T is the temperature of the LJ fluid, and U is the total potential. Dirichlet boundary conditions are applied on both the channel wall boundaries, i.e., on $\Gamma_1(x=0)$ and $\Gamma_2(x=L)$ (see Fig. 1),

$$c(x=0)=c_0,$$

$$c(x=L)=c_L. \tag{2}$$

The concentration of the LJ fluid at the channel walls is zero, i.e., $c_0=c_L=0$. Hence, in order to solve Eq. (1), an additional constraint has to be applied on the fluid concentration $c(x)$ inside the channel. Assuming that there is no mass transfer into or out of the channel, the average concentration of the LJ fluid atoms inside the channel will always be maintained. Hence, we impose a constraint on the concentration profile in the channel to ensure that the average concentration of the LJ fluid atoms inside the channel is c_{avg}, i.e.,

$$\frac{1}{L}\int_0^L c(x)dx=c_{\text{avg}}. \tag{3}$$

Typically, for large channels the concentration in the central part of the channel is close to the bulk value. In this case c_{avg} is specified to be the bulk concentration of the fluid, c_{bulk}. For smaller channels, the average concentration is typically smaller than the bulk concentration; this is discussed further in Sec. IV.

In summary, given the total potential profile $U(x)$ in the channel, one could obtain the concentration profile across the channel by solving Eq. (1) with boundary conditions and constraints given by Eqs. (2) and (3).

A. Models for the total potential $U(x)$

The total potential at a point x inside the channel, $U(x)$, depends on the concentrations of the wall and fluid atoms inside the channel as well as on the interatomic LJ force field of the wall and fluid atoms. $U(x)$ can thus be obtained by a summation of the fluid-fluid and the wall-fluid potential, i.e.,

$$U(x)=U_{\text{wall-fluid}}(x)+U_{\text{fluid-fluid}}(x). \tag{4}$$

1. The wall-fluid potential

The wall-fluid potential can be calculated from the integration of the contribution of a continuous distribution of wall atoms, as was originally discussed by Steele.[21,22] The wall-fluid potential at a point x, $U_{\text{wall-fluid}}(x)$, can be obtained by accounting for the interaction of an atom at a position x

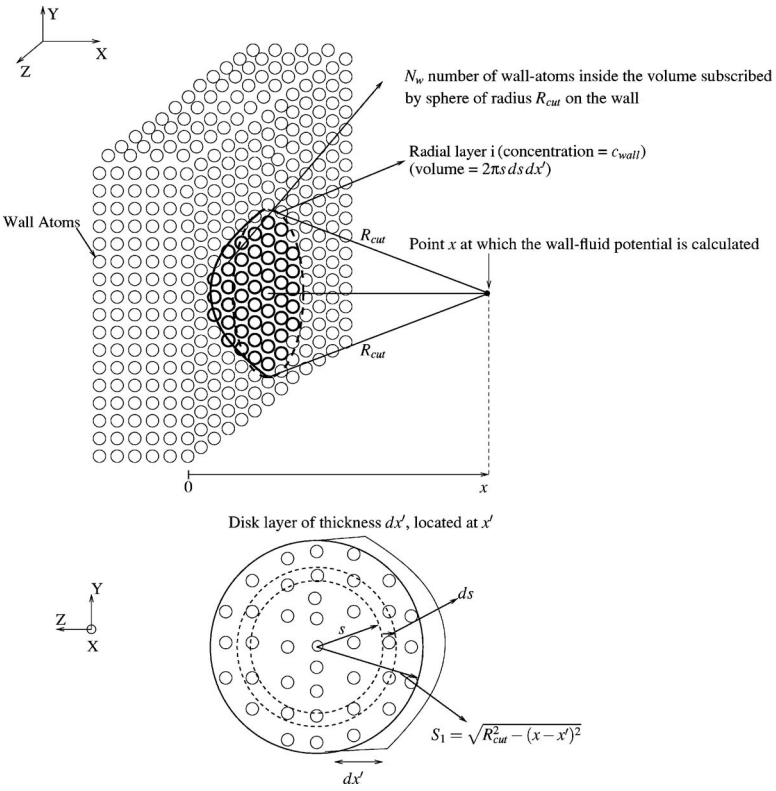

FIG. 2. The shaded region in the figure (top) is the volume circumscribed by the sphere of radius R_{cut} located at the point x with the channel wall. Figure (bottom) also shows the disk layer of thickness dx' and radius $\sqrt{R_{\text{cut}}^2-(x-x')^2}$ used for the purpose of integration of Eq. (8) in the circumscribed volume.

with all the wall atoms in the neighborhood of x by using the 12–6 LJ (Ref. 23) wall-fluid interatomic potential, i.e.,

$$u_{\text{LJ}}^{wf}(r) = \left[\frac{C_{12}^{wf}}{r^{12}} - \frac{C_6^{wf}}{r^6}\right], \tag{5}$$

where $C_{12}^{wf}=4\epsilon_{wf}\sigma_{wf}^{12}$ and $C_6^{wf}=4\epsilon_{wf}\sigma_{wf}^{6}$. ϵ_{wf} and σ_{wf} are the wall-fluid LJ energy and distance parameters, respectively. In the pairwise LJ interaction, the potential is negligible beyond a certain cutoff distance which is defined as R_{cut}. Let N_w be the number of wall atoms within a sphere of radius R_{cut} from the point x. The total wall-fluid potential at the point x using a molecular representation is then given by

$$U_{\text{wall-fluid}}(x) = \sum_{i=1}^{N_w} u_{\text{LJ}}^{wf}(|x-x_i|), \tag{6}$$

where x_i is the location of the wall atom i. Representing the wall atoms by a density, $c_{\text{wall}}(x_i)$, we can approximate the wall-fluid potential at the point x by

$$U_{\text{wall-fluid}}(x) = \sum_{i=1}^{N_l} u_{\text{LJ}}^{wf}(|x-x_i|)c_{\text{wall}}(x_i)\Delta\Omega_i, \tag{7}$$

where N_l denotes the number of radial wall layers that represent the wall atoms within the sphere of radius R_{cut}, $c_{\text{wall}}(x_i)$ is the density of the wall atoms in the ith radial layer, and $\Delta\Omega_i$ is the volume of the ith radial layer.

A continuum approximation for the discrete summation given in Eq. (7) is given by

$$U_{\text{wall-fluid}}(x) = \int_{\Omega} u_{\text{LJ}}^{wf}(|x-x'|)c_{\text{wall}}(x')d\Omega', \tag{8}$$

where Ω' is the volume of the wall atoms circumscribed by the sphere of radius R_{cut}. The circumscribed volume is shown as the shaded region in Fig. 2. To evaluate the integral in Eq. (8), we assume that the circumscribed volume is composed of circular disks located at x' with a thickness dx' (see Fig. 2). The wall-fluid potential at x due to a circular disk can be expressed as

$$dU_{\text{wall-fluid}}(x) = \left[\int_0^{S_1} u_{\text{LJ}}^{wf}(S)c_{\text{wall}}(x')2\pi s ds\right]dx', \tag{9}$$

where $S=\sqrt{s^2+(x-x')^2}$ and $S_1=\sqrt{R_{\text{cut}}^2-(x-x')^2}$. Since R_{cut} is used only for computational efficiency in MD simulations, a more accurate treatment is

$$dU_{\text{wall-fluid}}(x) = \left[\int_0^{\infty} u_{\text{LJ}}^{wf}(S)c_{\text{wall}}(x')2\pi s ds\right]dx'. \tag{10}$$

Assuming the walls are infinitely thick, the total wall-fluid potential due to the left wall can be rewritten as

$$U_{\text{wall-fluid}}(x) = \int_{-\infty}^{0} dU_{\text{wall-fluid}}dx'. \tag{11}$$

If the wall-fluid potential at the point x is influenced by both walls, then

$$U_{\text{wall-fluid}}(x) = \int_{-\infty}^{0} dU_{\text{wall-fluid}} dx' + \int_{L}^{\infty} dU_{\text{wall-fluid}} dx'. \tag{12}$$

If the wall-atom concentration c_{wall} is assumed to be uniform, the total wall-fluid potential $U_{\text{wall-fluid}}$ is then given by

$$U_{\text{wall-fluid}}(x) = c_{\text{wall}} \int_{-\infty}^{0} \int_{0}^{\infty} \left[\frac{C_{12}^{wf}}{S^{12}} - \frac{C_{6}^{wf}}{S^{6}} \right] 2\pi s ds dx' + c_{\text{wall}} \int_{L}^{\infty} \int_{0}^{\infty} \left[\frac{C_{12}^{wf}}{S^{12}} - \frac{C_{6}^{wf}}{S^{6}} \right] 2\pi s ds dx'. \tag{13}$$

Simplifying Eq. (13), the final expression for $U_{\text{wall-fluid}}$ at the position x is given by

$$U_{\text{wall-fluid}}(x) = \frac{2\pi C_{12}^{wf} c_{\text{wall}}}{90} \left[\frac{1}{x^9} + \frac{1}{(L-x)^9} \right] - \frac{2\pi C_{6}^{wf} c_{\text{wall}}}{12} \left[\frac{1}{x^3} + \frac{1}{(L-x)^3} \right]. \tag{14}$$

2. The fluid-fluid potential

In an atomistic approach, the fluid-fluid potential at a position x, $U_{\text{fluid-fluid}}(x)$, can be obtained by summing the interatomic fluid-fluid potential (u_{LJ}^{ff}) over all the fluid atoms surrounding the position x. The interatomic fluid-fluid potential u_{LJ}^{ff} is given by

$$u_{\text{LJ}}^{ff}(r) = \left[\frac{C_{12}^{ff}}{r^{12}} - \frac{C_{6}^{ff}}{r^{6}} \right], \tag{15}$$

where $C_{12}^{ff} = 4\epsilon_{ff}\sigma_{ff}^{12}$ and $C_{6}^{ff} = 4\epsilon_{ff}\sigma_{ff}^{6}$. ϵ_{ff} and σ_{ff} are the fluid-fluid LJ energy and distance parameters, respectively. Assuming that the LJ potential is negligible beyond a certain cutoff distance R_{cut} from the point x, $U_{\text{fluid-fluid}}$ is given by

$$U_{\text{fluid-fluid}}(x) = \sum_{i=1}^{N_f} u_{\text{LJ}}^{ff}(|x - x_i|), \tag{16}$$

where N_f is the number of fluid atoms within the sphere of radius R_{cut} from the point x. Representing the fluid atoms by a density, $c(x_i)$, we can approximate the fluid-fluid potential at a point x to be

$$U_{\text{fluid-fluid}}(x) = \sum_{i=1}^{N_m} u_{\text{LJ}}^{ff}(|x - x_i|) c(x_i) \Delta\Omega_i, \tag{17}$$

where N_m denotes the number of fluid layers representing the fluid atoms within the sphere of radius R_{cut}, $c(x_i)$ is the density of the fluid atoms in the ith radial fluid layer, and $\Delta\Omega_i$ is the volume of the ith radial layer. Similar to the calculation of the wall-fluid potential, the calculation of the potential from the fluid atoms can also be performed by using a continuum approach. The continuum approximation for the discrete summation given in Eq. (17) is

$$U_{\text{fluid-fluid}}(x) = \int_{\Omega'} u_{\text{LJ}}^{ff}(r) c(x') d\Omega', \tag{18}$$

where $r = |x - x'|$, Ω' is the volume circumscribed by the sphere of radius R_{cut} within the channel (excluding any volume that might be circumscribed on the channel walls). For the fluid layers within a distance of σ_{ff} from the point x, if we assume that c approximately obeys the Boltzmann distribution, then c has the form of $\exp(-u_{\text{LJ}}^{ff}/K_B T)$ (K_B is the Boltzmann constant). This indicates that the variation of r in the integrand of Eq. (18) is of the order of $O(r^{-24})$. This very high degree of r in the integrand will lead to numerical singularities when evaluating Eq. (18) for $r \to 0$. Hence, to calculate the fluid-fluid potential, we introduce a truncated soft-core LJ potential, $u_{\text{LJ}}^{t}(r)$, that consists of a modified functional form for the repulsive core of the 12–6 LJ potential. We define the functional form for $u_{\text{LJ}}^{t}(r)$ in a similar fashion to that used by Mezei[24] for free-energy calculations of dense LJ fluids. The expression for u_{LJ}^{t} is given by

$$u_{\text{LJ}}^{t}(r) = \begin{cases} 0 & r \le R_{\text{crit}} \\ \left[2 - \left(\dfrac{r}{R_{\text{min}}} \right)^2 \right]^4 u_{\text{LJ}}^{ff}(R_{\text{min}}) & R_{\text{crit}} < r \le R_{\text{min}} \\ \left(\dfrac{C_{12}^{ff}}{r^{12}} - \dfrac{C_{6}^{ff}}{r^{6}} \right) & R_{\text{min}} \le r \le R_{\text{cut}} \end{cases}, \tag{19}$$

where R_{min} is the distance within which the modified soft-core repulsion term exists and R_{crit} is the distance within which the interaction potential is assumed to be zero. It can be observed from Eq. (19) that $u_{\text{LJ}}^{t}(r)$ consists of a soft-core repulsive term and a zero potential region within an "inner" core close to $r=0$. Additionally, u_{LJ}^{t} is not singular at the point $r=0$. In this paper, we use $R_{\text{min}} = 0.939\sigma_{ff}$ and $R_{\text{crit}} = 0.29\sigma_{ff}$. These parameters were determined by matching the fluid-fluid potential for a large channel (e.g., in this paper we have used an $11\sigma_{ff}$ channel) with the fluid-fluid potential obtained from molecular dynamics simulations. Figure 3 shows the comparison of u_{LJ}^{ff} with u_{LJ}^{t} given by Eq. (19) for these R_{min} and R_{crit} values.

Substituting u_{LJ}^{t} instead of u_{LJ}^{ff} in Eq. (18), we obtain the total fluid-fluid potential given by

$$U_{\text{fluid-fluid}}(x) = \int_{\Omega'} u_{\text{LJ}}^{t}(r) c(x') d\Omega'. \tag{20}$$

As shown in Fig. 4, Eq. (20) is integrated by assuming circular disks of thickness dx' spanning the region Ω'. The total fluid-fluid potential can thus be rewritten as

$$U_{\text{fluid-fluid}}(x) = \int_{x-R_{\text{cut}}}^{x+R_{\text{cut}}} \left[\int_{0}^{\sqrt{R_{\text{cut}}^2 - r^2}} u_{\text{LJ}}^{t}(r,s) c(x') \times (2\pi s) ds \right] dx'. \tag{21}$$

It should be noted that the limits of integration for x' in Eq. (21) will change when the point x is closer than R_{cut} from one of the channel walls. Details regarding further simplification of Eq. (21) are provided in the Appendix.

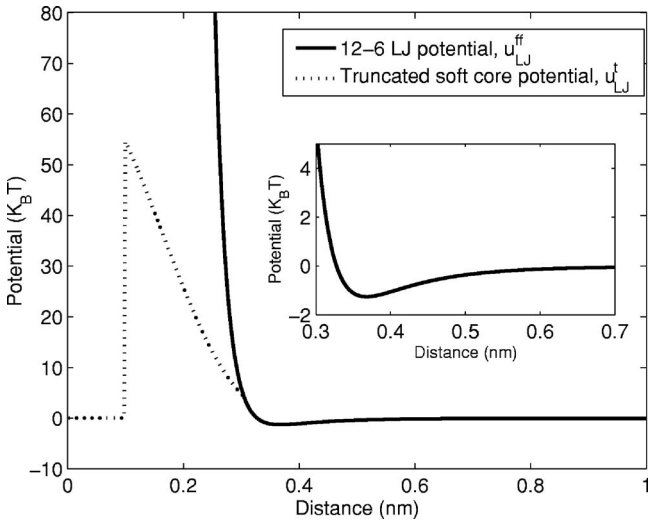

FIG. 3. The comparison between the interatomic 12–6 LJ fluid-fluid potential u^{ff}_{LJ} and the truncated soft-core LJ potential u^{t}_{LJ} used in the semiclassical formulation. The plot in the inset shows the variation of the attractive part of the potential in more detail.

B. Implementation

The semiclassical theory to compute the concentration of a LJ fluid sandwiched between two channels is given by Eq. (1), with boundary conditions given by Eqs. (2) and (3). The total potential, U, needed in Eq. (1) is given by Eq. (4). The contributions of the wall-fluid and fluid-fluid interactions to the total potential are computed by Eqs. (14) and (21), respectively. Since the fluid-fluid potential, $U_{\text{fluid-fluid}}$, is a function of the concentration of the fluid, c, Eq. (1) is nonlinear, and an iterative scheme needs to be used to find the self-consistent concentration and potential.

The implementation of the semiclassical approach is summarized in Algorithm 1. The input parameters needed for the implementation are the wall-fluid and the fluid-fluid LJ parameters, the average fluid concentration inside the channel c_{avg}, the concentration of the wall atoms, c_{wall}, and the length of the channel, L. The initial concentration of the fluid is assumed to be uniform throughout the channel with a value of c_{avg}. Given the concentration of the wall atoms, the wall-fluid potential can be computed using Eq. (14). Note that the wall-fluid potential needs to be computed only once as it does not depend on the concentration of the fluid. Using the initial guess for the fluid concentration, the fluid-fluid potential is computed using Eq. (21). Equation (1) is then solved to find the new fluid concentration. Since Eq. (1) is highly nonlinear, to obtain proper convergence we use a relaxation parameter, α, as shown in step 8 of Algorithm 1, to obtain the concentration during the iterative process. In this paper, we use $\alpha=0.65$. The iterative process is repeated until a self-consistent solution is obtained.

The proposed semiclassical approach can be easily applied to other geometries, e.g., nanopores. In addition, for geometries where the total potential varies not just along one dimension but along two or three dimensions, the semiclassical approach can be extended by considering a multidimensional form of Eq. (1).

Algorithm 1: The interatomic potential-based continuum formulation

(1) Input: LJ force field parameters for the wall $(\sigma_{wf}, \epsilon_{wf})$ and the fluid atoms $(\sigma_{ff}, \epsilon_{ff})$, relaxation parameter α, average concentration of the fluid, c_{avg}, concentration of LJ wall atoms, c_{wall}, and the channel width, L.

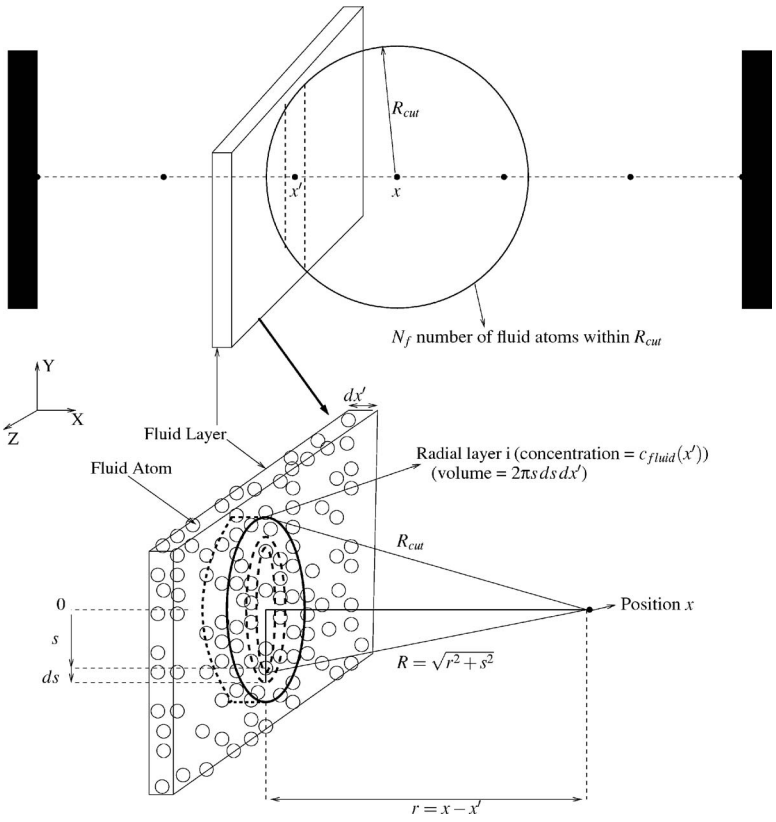

FIG. 4. A fluid layer located at x' is shown in the figure (top), along with the volume circumscribed by the sphere of radius R_{cut} on this layer. The circular disk of radius $\sqrt{R^2_{\mathrm{cut}}-r^2}$ and thickness dx' of this circumscribed volume is shown in the figure (bottom). The fluid-fluid potential due to this fluid layer on the point x is computed by integrating along the radius (s) and the thickness (r) of the layer.

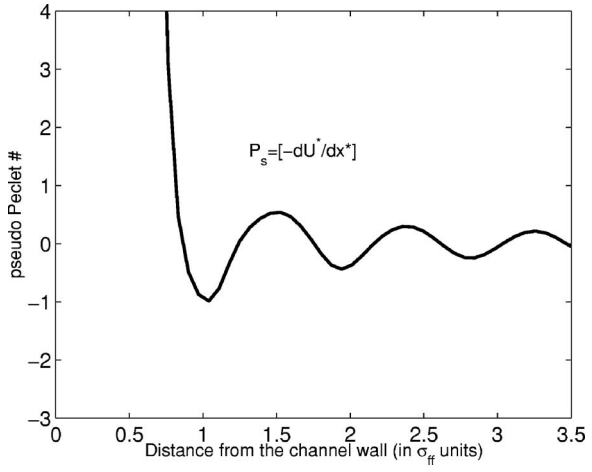

FIG. 5. The *pseudo*-Peclet number *Ps* across a channel of width $7\sigma_{ff}$ (only half the channel is shown).

(2) Set the initial guess, $c^0=c_{\text{avg}}$.
(3) Set counter $n=1$ and tolerance, tol (typically, tol$=1\times10^{-3}$).
(4) *Repeat*.
(5) Calculate $U^n_{\text{wall-fluid}}$ and $U^n_{\text{fluid-fluid}}$ from concentration c^{n-1} using Eqs. (14) and (21).
(6) $U^n=U^n_{\text{wall-fluid}}+U^n_{\text{fluid-fluid}}$.
(7) Using U^n, solve Eq. (1) with boundary conditions given by Eqs. (2) and (3) to obtain c^{new}.
(8) Perform relaxation step: $c^n=c^{n-1}+\alpha(c^{\text{new}}-c^{n-1})$,
(9) $n=n+1$.
(10) *Until* $|c^n-c^{n-1}|<\text{tol}$.
(11) The converged concentration (c^n) and potential profile (U^n) across the channel are obtained.

III. SIMULATION DETAILS

Equation (1) is normalized with respect to the channel width ($x^*=x/L$), the thermal energy ($U^*=U/RT$), and the bulk fluid concentration ($c^*=c/c_{\text{bulk}}$). The normalized equation is given by

$$\frac{d}{dx^*}\left(\frac{dc^*}{dx^*}\right)=\frac{d}{dx^*}(c^*P_s). \tag{22}$$

Here, the nondimensional parameter, P_s, is defined as the *pseudo*-Peclet number and is given by

$$P_s=-\frac{L}{RT}\frac{dU}{dx}. \tag{23}$$

Various numerical techniques can be used to solve Eq. (22); in this study we have used the finite volume method (FVM).[25] In Eq. (22), P_s is highly nonlinear close to the channel wall since the gradient of the potential can be high close to the channel wall region. The variation of P_s in a channel of width $L=7\sigma_{ff}$ is shown in Fig. 5. It can be observed from the figure that P_s is small in the center of the channel but has a significant nonlinear variation close to the channel wall. This nonlinear variation in P_s indicates that numerical stabilization techniques need to be used to solve Eq. (22). In this study, we have used the exponential numerical scheme to solve a convection-diffusion equation first proposed by Spalding.[26,27]

TABLE I. Parameters for the Lennard-Jones potential.

Pair	C_6(kJ nm^6 mol^{-1})	C_{12}(kJ nm^{12} mol^{-1})	σ (nm)
O-O	$0.261\,87\times10^{-2}$	$0.263\,07\times10^{-5}$	0.317
O-Si	$0.623\,37\times10^{-2}$	$0.769\,29\times10^{-5}$	0.3277
Si-Si	$0.147\,38\times10^{-1}$	$0.221\,91\times10^{-4}$	0.3385

The results obtained from semiclassical theory are compared with the results from MD. MD simulations are performed for a LJ fluid confined in a nanochannel as shown in Fig. 1 (top). The dimensions of the channel wall in the *y*- and *z*-directions are both 4.4 nm. The channel walls are made up of LJ atoms with the parameters of silicon obtained from the GROMOS force field.[28] The density of the channel walls is $c_{\text{wall}}=80$ atoms/nm^3. The walls consisted of six layers of silicon atoms with an interlayer spacing of 0.195 nm. The fluid inside the channel has the LJ parameters of the water-oxygen atoms from the SPC/E force field.[29] The bulk concentration of the LJ fluid inside the channel is $c_{\text{bulk}}=32$ atoms/nm^3. Table I gives the LJ force field used for the wall (silicon) and fluid (water-oxygen) atoms in our simulations studies. The time step for the *NVT* MD simulation was 2 fs and the LJ cutoff distance was 1.38 nm. The temperature of the fluid was maintained at 300 K during the simulation using a Nosé-Hoover thermostat,[30] with a time constant of 0.5 ps. The MD simulation was performed using GROMACS.[28] The range of channel widths used in the MD simulations was from $2\sigma_{ff}$ to $40\sigma_{ff}$.

IV. RESULTS

A. Comparison of the concentration and potential profiles

The accuracy of the semiclassical formulation was investigated by comparing the concentration and potential profiles obtained for different channel widths with those from MD simulations. The comparison of the concentration profiles for $11\sigma_{ff}$ channel is shown in Fig. 6. The average concentration used in the boundary condition given by Eq. (3) in the semiclassical formulation was the bulk fluid concentration, $c_{\text{avg}}=c_{\text{bulk}}=32$ atoms/nm^3 (corresponds to 55 M). The concentration profiles obtained from the MD simulation and the semiclassical formulation are found to be in good agreement. Both approaches predict a "bulklike" region in the channel center and the well-known "layering" of fluid near the wall. A total of 11 fluid concentration peaks are observed, and their magnitude diminishes while approaching the channel center. The location of the peaks is approximately σ_{ff} from each other. The concentration of the first peak from the channel wall is located between 0 and σ_{ff}, the second peak is located between σ_{ff} and $2\sigma_{ff}$, and so on till the center of the channel, making up the 11 peaks. The formation of the 11 peaks can be explained by investigating the total potential and its two components—wall-fluid and fluid-fluid potential as shown in Fig. 7. From the total potential it can be deduced that typically, the valley in the potential corresponds to the

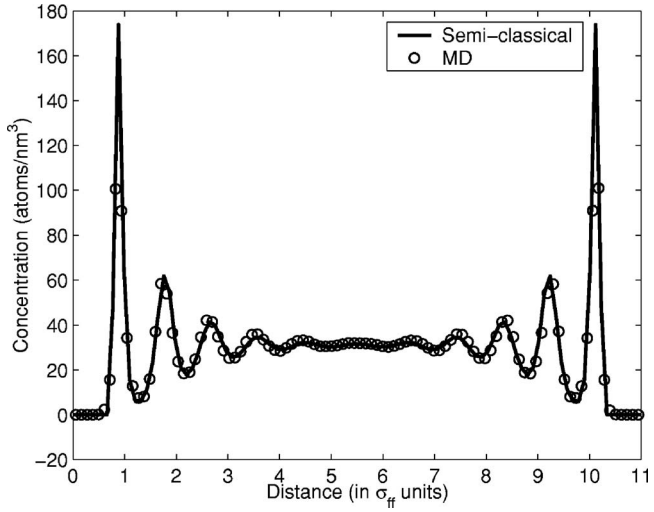

FIG. 6. Comparison of the density profile across an $11\sigma_{ff}$ channel obtained from MD simulation and the semiclassical formulation.

peak in the concentration, i.e., there are 11 valleys in the total potential corresponding to the 11 peaks in the concentration profile.

The total potential, U, has a valley in the region within σ_{ff} from the channel wall. As shown in Fig. 7 the wall-fluid potential, $U_{\text{wall-fluid}}$, also has a valley there while the fluid-fluid potential, $U_{\text{fluid-fluid}}$, has a positive peak. Thus, it can be deduced that the first valley in the total potential (corresponds to the first peak in the concentration) is primarily due to $U_{\text{wall-fluid}}$, while the $U_{\text{fluid-fluid}}$ acts to diminish this valley. Furthermore, the magnitudes of valleys in $U_{\text{fluid-fluid}}$ become less significant as we approach the center of the channel.

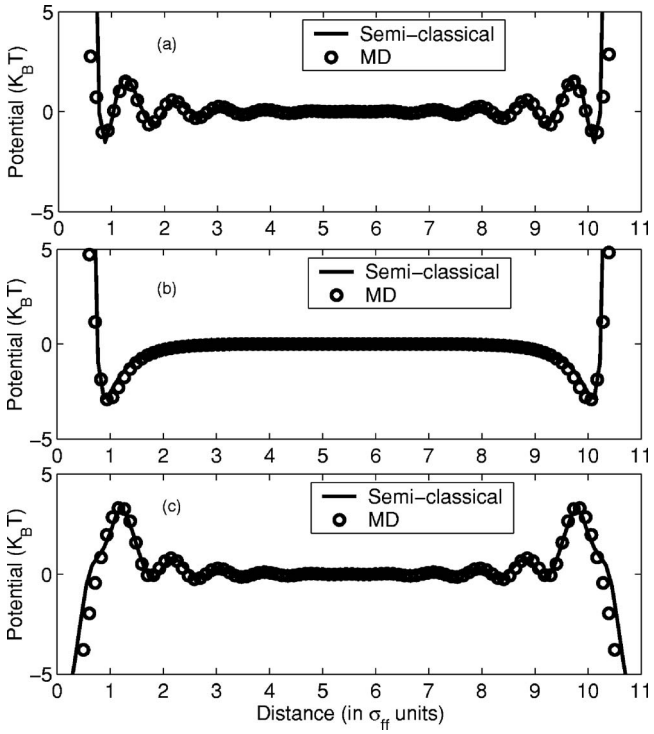

FIG. 7. Comparison of (a) the total potential; (b) the wall-fluid potential; and (c) the fluid-fluid potential, across an $11\sigma_{ff}$ channel obtained from MD simulations and the semiclassical formulation.

These valleys are responsible for the remaining nine peaks in the concentration profile. The wall-fluid potential also influences these peaks, but in a less significant manner and only within $4\sigma_{ff}$ from the channel wall. The valleys in the fluid-fluid potential do not exactly correspond with the valleys in the total potential because of the contribution from the wall-fluid potential.

It is observed that there is difference in the first peak of the concentration obtained from MD and semiclassical formulation. The first peak obtained from MD simulation is 105 atoms/nm^3, while that from the semiclassical formulation is 175 atoms/nm^3. This difference originates from the small difference in the total potential, U, within a distance σ_{ff} from the channel wall as shown in Fig. 7. This difference in U is due to both the $U_{\text{wall-fluid}}$ and the $U_{\text{fluid-fluid}}$. Within σ_{ff} from the wall, the valley of the $U_{\text{wall-fluid}}$ potential from the semiclassical formulation has a smaller magnitude as compared to the MD data. If the difference in U is dominated by $U_{\text{wall-fluid}}$, then the first peak in the concentration from the semiclassical formulation will be smaller than that from the MD simulation—contrary to the observation in the concentration profile. However, the $U_{\text{fluid-fluid}}$ potential is also found to influence this difference. $U_{\text{fluid-fluid}}$ from the semiclassical formulation is lower than the $U_{\text{fluid-fluid}}$ data from MD at the position of the first concentration peak ($\approx 0.9\sigma_{ff}$ from the wall). The combined effect of the $U_{\text{fluid-fluid}}$ (with a difference of $-0.4K_BT$ in potential as compared to MD) and $U_{\text{wall-fluid}}$ (with a difference of $0.05K_BT$ in potential as compared to MD) results in the magnitude of total potential, U, being larger for the semiclassical formulation, i.e., a more negative potential. Assuming that the concentration and the total potential obey the Boltzmann distribution, the first concentration peak observed from the semiclassical formulation is higher than that from the MD simulation. The difference in the $U_{\text{fluid-fluid}}$ potential could be due to the truncated soft-core potential introduced in Eq. (19). Though the truncated potential works well for bulk systems, it may not capture all the features in the interfacial region, leading to the deviation in $U_{\text{fluid-fluid}}$. Especially closer to the wall, i.e., $<0.7\sigma_{ff}$ from the wall, the deviation between the semiclassical and MD data in $U_{\text{fluid-fluid}}$ is significant. However, this deviation has a negligible influence on the converged solution (concentration) because the concentration itself is negligible in this region due to the large value in $U_{\text{wall-fluid}}$ and subsequently in U.

Further comparisons of the concentration and potential profiles were performed on channels with smaller widths. The concentration profiles obtained from MD and the semiclassical formulation are in good agreement in the case of the $7\sigma_{ff}$ wide channel. Since there is no "bulk" region in this case, the value of c_{avg}, which is also used in the semiclassical formulation, will be less than the bulk concentration, c_{bulk}. To enable proper comparison with MD simulations, c_{avg} was evaluated from the total number of atoms in the channel in the MD simulation divided by the volume of the channel region. In this channel, the volume of the channel is found to be 430 nm^3 ($7\sigma_{ff} \times 4.4$ nm $\times 4.4$ nm) and the number of fluid atoms in the channel in MD was 1285. Hence, the average fluid concentration is evaluated as $c_{\text{avg}} = 30$ atoms/nm^3. Figure 8 shows the comparison of the con-

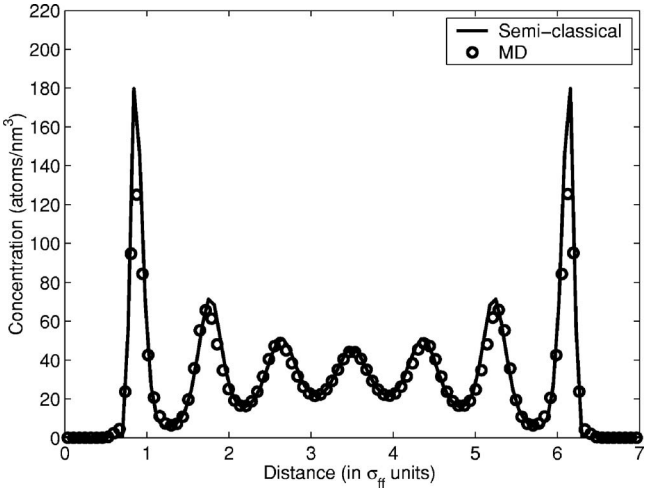

FIG. 8. Comparison of the density profile across a $7\sigma_{ff}$ channel obtained from MD and the semiclassical formulation.

centration profile obtained from both approaches. Consistent with the observations in the $11\sigma_{ff}$ channel, seven concentration peaks are observed in the $7\sigma_{ff}$ channel. The total potential, wall-fluid, and the fluid-fluid potential are shown in Fig. 9. The difference in the first peak in the concentration profile can again be explained using the wall-fluid and fluid-fluid potential, as was done in the case of the $11\sigma_{ff}$ channel.

B. Comparison in very small channels

The concentration and potential profiles obtained from MD and semiclassical formulations compare reasonably well even in smaller channels for widths ranging from $2\sigma_{ff}$ to $6\sigma_{ff}$. The comparison of the concentration profile in the $3\sigma_{ff}$ channel is shown in Fig. 10. Similar to the $7\sigma_{ff}$ channel, to make proper comparison between MD and semiclassical theory results, the value of c_{avg} for the $3\sigma_{ff}$ channel was calculated from the number of atoms used in the MD simulation and the value is 26 atoms/nm^3. The semiclassical formulation shows a good agreement with the MD data except for the first peak. The magnitude of the peak closer to the wall is higher with the semiclassical formulation compared to the MD data. Again, this difference can be explained from the potentials in the channel. The comparison of the total potential, wall-fluid, and fluid-fluid potential obtained from MD and semiclassical formulation are shown in Fig. 11.

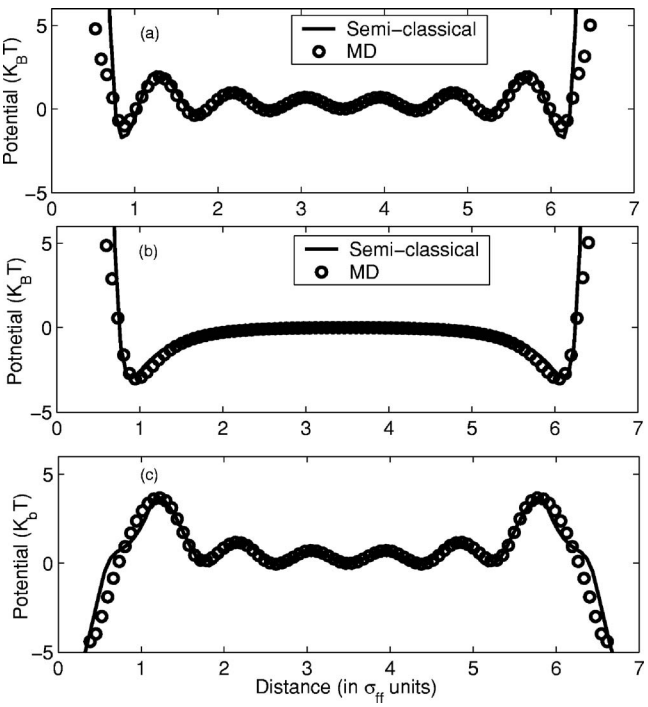

FIG. 9. Comparison of (a) the total potential; (b) the wall-fluid potential; and (c) the fluid-fluid potential, across a $7\sigma_{ff}$ channel from MD and semiclassical simulation.

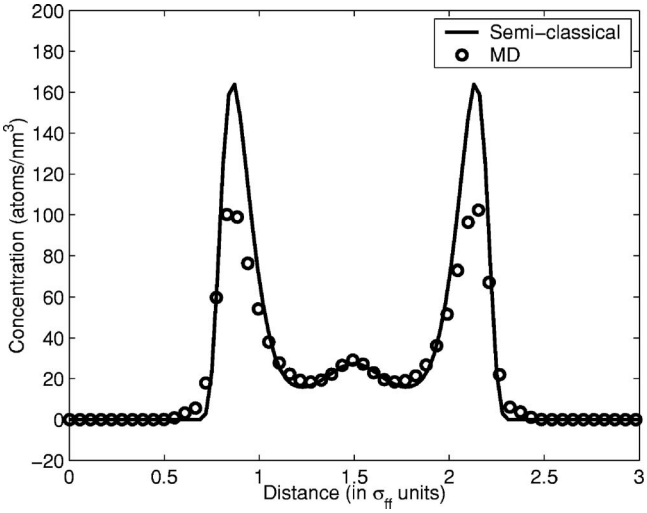

FIG. 10. The concentration profile in a $3\sigma_{ff}$ channel obtained from MD and semiclassical simulation.

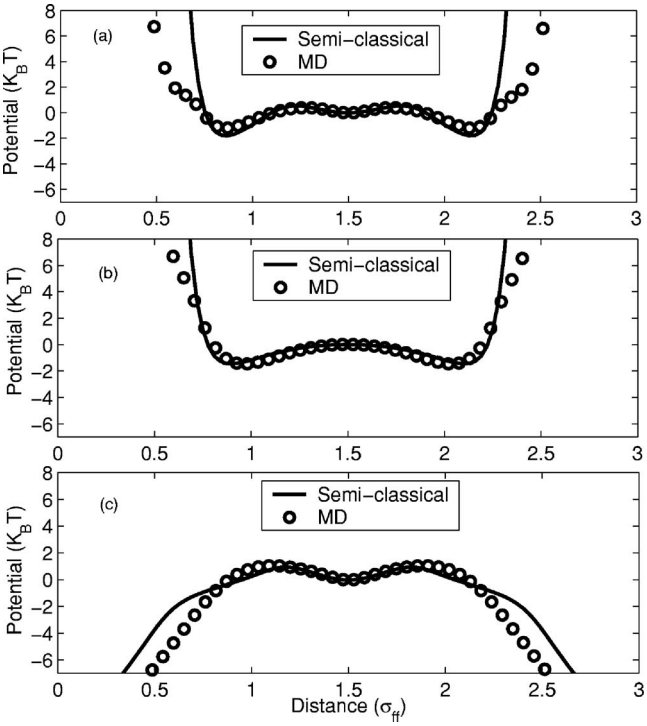

FIG. 11. Comparison of (a) the total potential; (b) the wall-fluid potential; and (c) the fluid-fluid potential in a $3\sigma_{ff}$ channel obtained from MD and semiclassical simulations.

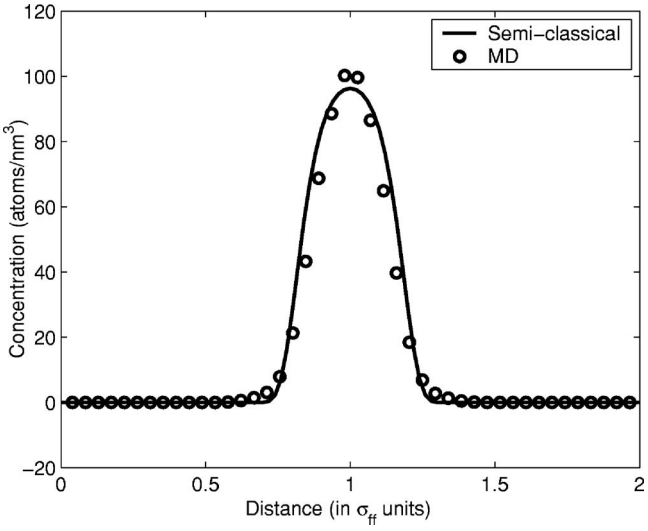

FIG. 12. The concentration profile in a $2\sigma_{ff}$ channel obtained from MD and the semiclassical simulations.

Similar to the observation for the $11\sigma_{ff}$ case, the wall-fluid potential from semiclassical formulation is higher at the first concentration peak as compared to the MD data, and the fluid-fluid potential from semiclassical formulation is lower than MD data at the same location. Higher difference in fluid-fluid potential leads to a lower value for the first valley of the combined total potential. Hence, the corresponding concentration peak is overestimated by the semiclassical formulation. The considerable deviation of the fluid-fluid potential even closer to the wall ($<0.7\sigma_{ff}$) and its negligible impact on the calculated concentration profile is similar to that observed and explained for the $11\sigma_{ff}$ channel. In addition, we observe that the concentration peak at the center of the channel is much diminished as compared to the peak at the center in the $7\sigma_{ff}$ channel. This observation is because of two reasons. First, the region available for the fluid molecules is typically the region $\sigma_{wf}<x<L-\sigma_{wf}$. In the $3\sigma_{ff}$ case, this region is about σ_{ff}. Hence, there does not exist enough room in the central region for the formation of a significant fluid layer. Second, the wall-fluid potential from channel walls on either side overlap, i.e., the wall-fluid potential at the center of the channel is considerable due to the contribution from the channel walls on either side [see Fig. 11(b)]. This wall-fluid potential overlap also prevents the formation of a significant concentration peak at the center of the channel. From the above discussion, it can be concluded that the semiclassical formulation is quite successful in predicting the fluid concentration in the channel even when the size of the central region is only about σ_{ff}.

As we further shrink the size of the channel width to $2\sigma_{ff}$, we still observe a good match for the concentration profile (see Fig. 12). The concentration was much smaller than the bulk concentration and, using the procedure outlined earlier, $c_{avg}=16$ atoms/nm^3 was obtained and used in the semiclassical formulation. Consistent with the trend in bigger channels, one would expect two concentration peaks in the $2\sigma_{ff}$ channel. However, the number of peaks obtained is one, not two. The reason for this is apparent from the analysis of the total potential, wall-fluid potential, and fluid-fluid potential (see Fig. 13). The wall-fluid potential overlap from the channel wall on either side becomes even larger than that in the case of the $3\sigma_{ff}$ channel. Thus, there is no attractive region (negative potential region) in the wall-fluid potential throughout the channel [see Fig. 13(b)]. Equation (14) still predicts a reasonable match for the wall-fluid potential with the MD data. Unlike in the higher channel width cases, as there exists only one valley in the wall-fluid potential, it contributes to only one concentration peak. The fluid-fluid potential has no valley and thus does not contribute to the formation of another concentration peak. Our semiclassical formulation has successfully captured this phenomenon and reasonably matches the concentration profile obtained from the MD simulation. There still exists a difference in the fluid-fluid potential calculated from MD and semiclassical formulations very close to the channel wall. The reason that this deviation does not affect the obtained concentration profiles is the same as explained in the $3\sigma_{ff}$ channel case. It should be noted that a more accurate calculation of the wall-fluid potential in all these channel widths would involve accounting for the discreteness of the channel wall. Also, $2\sigma_{ff}$ was the smallest channel through which fluid atoms enter in a MD simulation. In a $1\sigma_{ff}$ channel, fluid atoms hardly enter the channel, since there is a strong repulsion by the LJ potential from both walls.

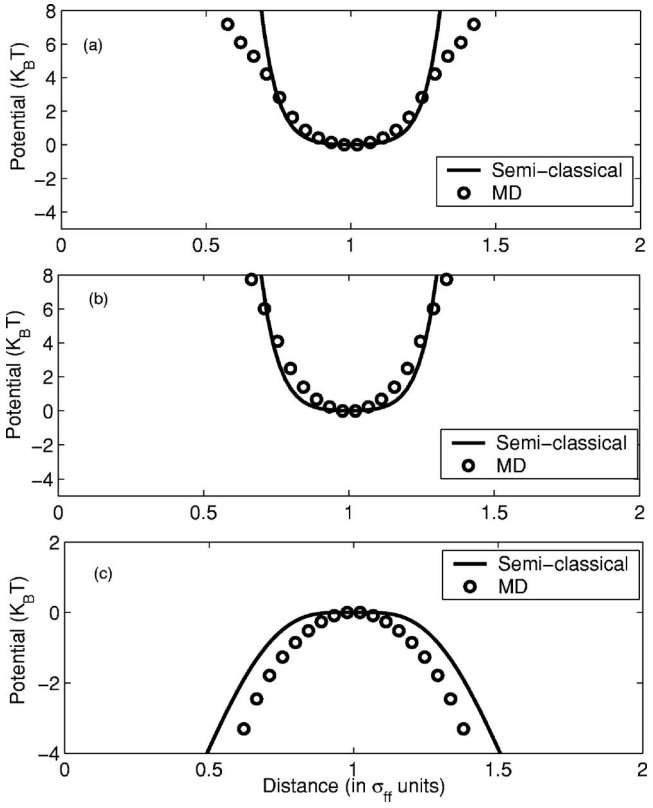

FIG. 13. Comparison of (a) the total potential; (b) the wall-fluid potential; and (c) the fluid-fluid potential obtained from MD and semiclassical simulations in a $2\sigma_{ff}$ channel.

C. Semiclassical theory predictions in large channels

The concentration profiles obtained from the semiclassical formulation and MD are in good match for a relatively

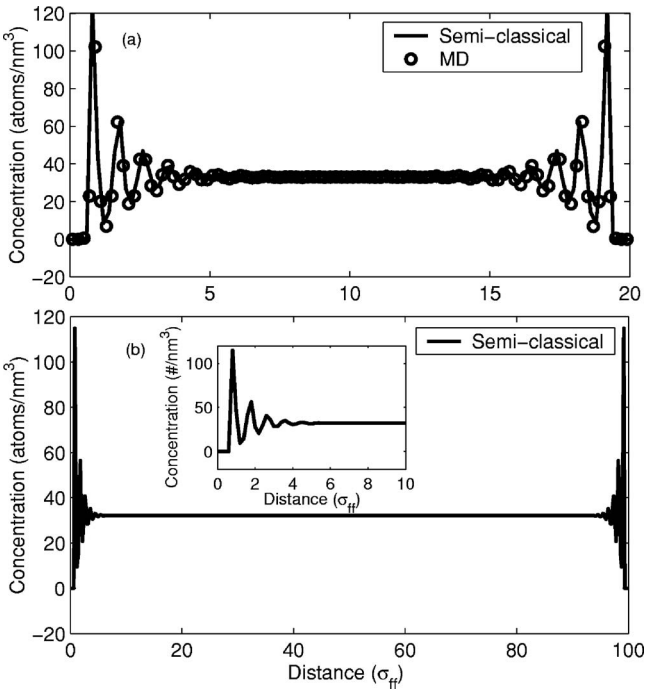

FIG. 14. The concentration profile of the LJ fluid (a) in a $20\sigma_{ff}$ wide channel obtained from MD and semiclassical formulation, and (b) in a $100\sigma_{ff}$ wide channel obtained from the semiclassical simulation. The inset in (b) shows the "layering" in the concentration profile close to the channel wall region.

large channel of width $20\sigma_{ff}$, as shown in Fig. 14(a). For an even larger channel, e.g., a $100\sigma_{ff}$ channel, the MD simulation is computationally expensive. However, even for such a big channel, the atomistic features in the interfacial region can be significant. Although a lot of work has gone into developing a model/formulation to capture the atomistic features with a very low computing cost for very large channels, it has yet to be successful. The semiclassical formulation that has been proposed here has been successful in this regard. Figure 14(b) shows the concentration obtained from the semiclassical formulation for this large channel. As shown in the figure (inset), both the "layering" of the fluid very close to the wall and the bulk concentration at the center of the channel are captured using the semiclassical formulation. The number of concentration peaks that can be observed is much smaller than 100, since the peaks diminish to the bulk concentration within a distance of $10\sigma_{ff}$ from the channel wall. It is apparent that using a relatively inexpensive semiclassical computation, one could obtain the concentration and potentials in $100\sigma_{ff}$ or even higher channel widths. Hence, the semiclassical formulation can be used for fast computations involving very large channels without any loss in the atomistic detail close to the wall-fluid interface.

V. CONCLUSIONS

In this work, an interatomic potential-based semiclassical theory has been proposed to predict the concentration and potential profiles of a LJ fluid confined between two channel walls. The proposed formulation solves the Nernst-Planck equation, using a potential obtained from an atomistic description. While the wall-fluid potential was calculated from the 12–6 LJ potential, the fluid-fluid potential is evaluated by introducing a truncated soft-core LJ atomistic potential. It is observed that the concentrations and potentials predicted by the semiclassical theory are in good agreement with the MD simulations for all the channel widths studied—ranging from $2\sigma_{ff}$ to $20\sigma_{ff}$—thus validating the accuracy of the formulation. The formulation can be further improved by developing more advanced models for the wall-fluid and coarse-grained approaches for the fluid-fluid potential. The semiclassical approach provides a means to capture the underlying atomistic physics in the interfacial region without resorting to computationally intensive atomistic simulations. Further, the semiclassical formulation was used to capture the interfacial behavior in a very large $100\sigma_{ff}$ channel, for which MD simulation is computationally much more expensive. The ease of implementation and the robustness of the approach make it unique to ascertain the static fluid properties at scales ranging from the macroscale to a few atomic diameters.

ACKNOWLEDGMENTS

This work was supported by NSF under Grant Nos. 0120978, 0328162, 0523435, 0625421 and by NIH under Grant No. PHS 2 PN2 EY016570B.

APPENDIX: DETAILED FORMULATION OF THE FLUID-FLUID POTENTIAL

To obtain the detailed fluid-fluid potential, we substitute u^t_{LJ} from Eq. (19) into Eq. (21) and ensure the appropriate limits for the integration when the point x is close to the channel wall. Integrating out the inner integral, $U_{\text{fluid-fluid}}$ becomes

$$\begin{aligned} U_{\text{fluid-fluid}}(x) = &\int_{x}^{x+R_{\text{crit}}} [f(R_{\text{crit}}) + g(R_{\min})]c(x')dx' \\ &+ \int_{x+R_{\text{crit}}}^{x+R_{\min}} [f(r) + g(R_{\min})]c(x')dx' \\ &+ \int_{x+R_{\min}}^{x+R_{cut}} [f(R_{\min}) + g(r)]c(x')dx' \\ &+ \int_{x-R_{\text{crit}}}^{x} [f(R_{\text{crit}}) + g(R_{\min})]c(x')dx' \\ &+ \int_{x-R_{\min}}^{x-R_{\text{crit}}} [f(r) + g(R_{\min})]c(x')dx' \\ &+ \int_{x-R_{\text{cut}}}^{x-R_{\min}} [f(R_{\min}) + g(r)]c(x')dx'. \end{aligned} \tag{A1}$$

Here, the functions f and g are defined as

$$f(p) = \frac{\pi R^2_{\min} u^{ff}_{\mathrm{LJ}}(R_{\min})}{5}\left\{\left[2 - \left(\frac{p}{R_{\min}}\right)^2\right]^5 - 1\right\};$$

$$0 \le p < R_{\min}, \tag{A2}$$

and

$$g(p) = \frac{\pi C_{12}^{ff}}{5}\left(\frac{1}{p^{10}} - \frac{1}{R_{\text{cut}}^{10}}\right) - \frac{\pi C_{6}^{ff}}{2}\left(\frac{1}{p^{4}} - \frac{1}{R_{\text{cut}}^{4}}\right);$$

$$R_{\text{min}} \leq p \leq R_{\text{cut}}. \tag{A3}$$

The notation in the above equations is the same as that given in Eqs. (19) and (21).

[1] T. Thorsen, S. J. Maerkl, and S. R. Quake, Science **298**, 580 (2002).
[2] J. L. Perry and S. G. Kandlikar, Microfluid. Nanofluid. **2**, 185 (2006).
[3] B. van der Bruggen, C. Vandecasteele, T. V. Gestel, W. Doyen, and R. Leysen, Environ. Prog. **22**, 46 (2003).
[4] G. E. Karniadakis, A. Beskok, and N. R. Aluru, *Microflows and Nanoflows: Fundamentals and Simulation* (Springer, New York, 2005).
[5] D. Frenkel and B. Smith, *Understanding Molecular Simulation* (Academic, New York, 2001).
[6] R. Qiao and N. R. Aluru, J. Chem. Phys. **118**, 4692 (2003).
[7] S. Attinger and P. Koumoutsakos, *Multiscale Modelling and Simulation* (Springer, Berlin, 2004).
[8] E. Weinan and B. Engquist, Commun. Math. Sci. **1**, 87 (2003).
[9] J. Li, D. Liao, and S. Yip, J. Comput.-Aided Mater. Des. **6**, 95 (1999).
[10] R. Qiao and N. R. Aluru, Int. J. Multiscale Comp. Eng. **2**, 173 (2004).
[11] F. Müller-Plathe, ChemPhysChem **3**, 754 (2002).
[12] S. Izvekov and G. A. Voth, J. Chem. Phys. **123**, 134105 (2005).
[13] P. Hoogerbrugge and J. M. V. A. Koelman, Europhys. Lett. **19**, 155 (1992).
[14] R. D. Groot and P. B. Warren, J. Chem. Phys. **107**, 4423 (1997).
[15] I. Vattulainen, M. Karttunen, G. Besold, and J. M. Polson, J. Chem. Phys. **116**, 3967 (2002).
[16] I. V. Pivkin and G. E. Karniadakis, Phys. Rev. Lett. **96**, 206001 (2006).
[17] Y. Tang, A. Tong, and B. C.-Y. Lu, Fluid Phase Equil **134**, 21 (1997).
[18] J. Wu and Z. Li, Annu. Rev. Phys. Chem. **58**, 85 (2007).
[19] *Density Functionals in the Theory of Nonuniform Fluids*, edited by D. Henderson (Marcel Dekker, New York, 1992).
[20] T. Teorell, Prog. Biophys. Biophys. Chem. **3**, 305 (1953).
[21] W. A. Steele, *Interaction of Gases with Solid Surfaces* (Pergamon, New York, 1974).
[22] W. A. Steele, J. Phys. Chem. **82**, 817 (1978).
[23] J. E. Lennard-Jones, Proc. Phys. Soc. **43**, 461 (1931).
[24] M. Mezei, Mol. Simul. **2**, 201 (1989).
[25] J. M. Hyman, R. J. Knapp, and J. C. Scovel, Physica D. **60**, 112 (1992).
[26] D. B. Spalding, Int. J. Numer. Methods Eng. **4**, 551 (1972).
[27] S. V. Patankar, *Numerical Heat Transfer and Fluid Flow* (McGraw-Hill, New York, 1980).
[28] E. Lindahl, B. Hess, and D. van der Spoel, J. Mol. Model. **7**, 306 (2001).
[29] S. Koneshan, J. C. Rasaiah, R. M. Lynden-Bell, and S. H. Lee, J. Phys. Chem. B **102**, 4193 (1998).
[30] S. Nosé, J. Chem. Phys. **81**, 511 (1984).